JASA ARTICLE

Multiple constraint matched field processing tolerant to array tilt mismatch

Gihoon Byun,[a] F. Hunter Akins, Kay L. Gemba,[b] H. C. Song, and W. A. Kuperman
Scripps Institution of Oceanography, La Jolla, California 92093-0238, USA

ABSTRACT:
A multiple constraint method (MCM) specifically designed to accommodate the uncertainty of array tilt is developed for matched field processing (MFP). Combining the MCM with the white noise gain constraint method results in a processor that is tolerant to both array tilt and environmental mismatch. Experimental results verify the robustness of the proposed MFP to localize and track a surface ship radiating broadband noise (200–500 Hz), using a 56-m long vertical array with tilt in approximately 100-m deep shallow water. © *2020 Acoustical Society of America*.
https://doi.org/10.1121/10.0000784

(Received 15 August 2019; revised 3 February 2020; accepted 4 February 2020; published online 25 February 2020)
[Editor: Stan E. Dosso] Pages: 1231–1238

I. INTRODUCTION

The purpose of this paper is to present an adaptive matched field processor (MFP) that is tolerant to both environmental mismatch and array tilt mismatch. MFP, a model-based approach for solving inverse problems by comparing acoustic data with solutions of the wave equation (replicas), has been developed for localizing underwater acoustic sources.[1,2] While the conventional, linear Bartlett beamformer is tolerant of environmental mismatch, it has significant problems with sidelobes that are often indistinguishable from the mainlobe.[3] In contrast, the adaptive beamformer based on Capon's minimum variance (MV) provides excellent sidelobe control and a high resolution.[4,5] The high-resolution feature is usually considered an advantage, but increases the sampling requirements that would lead to substantial numerical efforts to evaluate the replica field. The high resolution at high signal-to-noise ratios (SNRs) also makes the MV highly sensitive to environmental parameters, requiring accurate knowledge of the ocean-acoustic environment.[3]

To avoid sampling problems and environmental model sensitivity, a white noise gain constraint (WNC) has been developed which effectively increases the mainlobe width while maintaining its sidelobe control.[6–8] The widening of the mainlobe induces a widening in other significant parameters as well, yielding less sensitivity to environmental mismatch.[3] On the other hand, Krolik applied the MV beamformer with multiple constraints method (MCM) to achieve greater robustness in a random ocean channel, which is based on an ensemble of perturbations in sound speed profiles (SSPs)[5] or entire environmental parameters[9] spanning a range of possible wave-front perturbations. Similarly, Kim *et al.*[10] adopted multiple frequency constraints based on the waveguide invariant theory and demonstrated robust time-reversal focusing in a fluctuating environment due to internal waves.

This paper will address a surprisingly neglected source of mismatch—array tilt induced by ocean currents. As reported in our recent paper,[11] even a small tilt angle (e.g., 2°) in shallow water has a devastating impact on the more robust Bartlett beamformer if not compensated for. Despite the sensitivity, there has not been much work on the array tilt in the MFP literature.[12,13] One way to address the issue is to include the array tilt in the source parameter space (range and depth), resulting in a computationally intensive three-dimensional parameter search.[2] Alternatively, Schmidt *et al.*[3] applied an environmentally tolerant MCM to the case involving a small array tilt with limited success, where the multiple point constraints were constructed to achieve a mainlobe response equal to the Bartlett beamformer, similar to the WNC. In this paper, we propose a MCM specifically designed to accommodate the uncertainty of the array tilt, referred to as multiple tilt constraints (MTC). The basic idea is to broaden the boundaries of the array geometry via MTC while widening the mainlobe via WNC. The resulting adaptive MFP that combines the MTC and the WNC can be tolerant to both array tilt and moderate environmental mismatch, which will be demonstrated using simulations and at-sea experimental data.

In Sec. II, we first review the conventional Bartlett MFP and then derive a MCM (i.e., MTC) processor that is tolerant of array tilt, followed by the WNC that provides additional robustness to some environmental mismatch while still suppressing sidelobes. Section III revisits a recent shallow water experiment (SAVEX15),[11] where a 56-m long, bottom-moored vertical array recorded the ship noise (200–500 Hz) from the R/V *Onnuri* circling around the array in approximately 100-m deep shallow water. Section IV presents simulation results of various MFP processors for a source frequency of 200 Hz in the presence of parameter mismatch such as sound speed, array tilt, and grid sampling. In Sec. V, a representative example from the SAVEX15 experiment is analyzed in detail, and then the overall

[a]Electronic mail: gbyun@ucsd.edu
[b]Present address: Naval Research Laboratory, Washington, D.C. 20375, USA

performance of tracking the ship during the entire 4-h event is described. A concluding remark is given in Sec. VI.

II. MFPS

A. Conventional Bartlett MFP

Let $\mathbf{x}$ denote the column vector of complex narrowband array output in a particular frequency bin (f) for a source at range and depth (r_s, z_s). The Bartlett beamformer output power, P_{B}, is given by

$$P_{\mathrm{B}}(r,z;f) = \mathbf{w_B}^{\dagger}(r,z,f)\mathbf{R}(r_s,z_s,f)\mathbf{w_B}(r,z,f), \tag{1}$$

where $\mathbf{w}_B(r,z)$ is the Bartlett beamformer weight vector, and $\mathbf{R} = E\{\mathbf{x}\mathbf{x}^{\dagger}\}$ is the ensemble covariance matrix where E denotes expectation and superscript † denotes complex conjugate transpose. The function $P_{\mathrm{B}}(r,z)$ is also called the ambiguity surface of the beamformer. In practice, the data vectors are averaged to form the sample covariance matrix[1]

$$\hat{\mathbf{R}}(f) = \frac{1}{L}\sum_{l=1}^{L}\mathbf{x}_l(f)\mathbf{x}_l^{\dagger}(f), \tag{2}$$

where L is the number of snapshots and $\mathbf{x}_l(f)$ are snapshots of time samples and frequency bins obtained by a fast Fourier transform (FFT) on a windowed data segment along the array.

In Eq. (1), the Bartlett weight vector, $\mathbf{w}_B(r,z)$, is a normalized version of the replica vector, $\mathbf{e}(r,z)$, based on an acoustic environmental model calculated at the array for a harmonic point source (f) positioned at (r, z),

$$\mathbf{w}_B(r,z;f) = \frac{\mathbf{e}(r,z,f)}{||\mathbf{e}(r,z,f)||}. \tag{3}$$

For broadband signals, the narrowband beamformer output of Eq. (1) can be incoherently averaged across the signal bandwidth. To simply notation, the frequency variable f will be dropped for the remainder of this section.

B. MCM derivation

The adaptive MCM weight vector, $\mathbf{w}_A(r,z)$, is to minimize the output power subject to multiple linear equality constraints,

$$\min_{\mathbf{w_A}} \mathbf{w_A^{\dagger}}\mathbf{R}\mathbf{w}_A \quad \text{subject to } \mathbf{w_A^{\dagger}}\mathbf{E} = \mathbf{d}. \tag{4}$$

The well-known solution to this multi-constraint beamformer is derived using Lagrangian multipliers,[3]

$$\mathbf{w}_A = \mathbf{R}^{-1}\mathbf{E}\left[\mathbf{E}^{\dagger}\mathbf{R}^{-1}\mathbf{E}\right]^{-1}\mathbf{d}^{\dagger}, \tag{5}$$

where $\mathbf{E}$ is the replica matrix as composed of M replica vectors for the M constraints. Thus for an N-element array, $\mathbf{E}$ is an $N \times M$ complex matrix ($M < N$), and $\mathbf{d}$ is the constraint response (row) vector ($1 \times M$). If there is only a single constraint in the look direction (i.e., $M = 1$), $\mathbf{w}_A$ reduces to the adaptive MV beamformer.

The choice of the constraints is not obvious, but one natural set of constraints is to make the MCM response equal to that of Bartlett beamformer in the look direction within the Bartlett mainlobe (i.e., local Bartlett behavior and global MV behavior).[3,5] Instead of widening the mainlobe, our choice for multiple constraints to accommodate the uncertainty of the array tilt is to broaden the boundaries of the array geometry for the same look direction (r, z),

$$\mathbf{E} = \left[\frac{\mathbf{e}_{\Delta\theta_1^+}}{||\mathbf{e}_{\Delta\theta_1^+}||}, \ldots, \frac{\mathbf{e}_{\Delta\theta_m^0}}{||\mathbf{e}_{\Delta\theta_m^0}||}, \ldots, \frac{\mathbf{e}_{\Delta\theta_M^-}}{||\mathbf{e}_{\Delta\theta_M^-}||}\right], \tag{6}$$

where the column vectors $\mathbf{e}_{\Delta\theta}$ denote the replica field for various tilt angles chosen symmetrically, as depicted in Fig. 1, with respect to the no-tilt case of $\Delta\theta_m^0 = 0°$ in the middle (thick vertical line), i.e., $m = (M+1)/2$. The normalized column vectors are consistent with the conventional Bartlett weight vector, $\mathbf{w}_B$.

Similar to the MCM implemented with the natural constraints,[3] here we choose the corresponding response (row) vector $\mathbf{d}$ as

$$\mathbf{d} = \left[\frac{\mathbf{e}^{\dagger}_{\Delta\theta_m^0}\mathbf{e}_{\Delta\theta_1^+}}{||\mathbf{e}_{\Delta\theta_m^0}||\,||\mathbf{e}_{\Delta\theta_1^+}||}, \ldots, 1, \ldots, \frac{\mathbf{e}^{\dagger}_{\Delta\theta_m^0}\mathbf{e}_{\Delta\theta_M^-}}{||\mathbf{e}_{\Delta\theta_m^0}||\,||\mathbf{e}_{\Delta\theta_M^-}||}\right], \tag{7}$$

i.e., the inner product of the no-tilt replica (middle), $\mathbf{e}_{\Delta\theta_m^0}$, and the replica in the tilt constraint point, $\mathbf{e}_{\Delta\theta}$, yielding the unity gain constraint for no array tilt (i.e., $d_m = 1$). Since the multiple constraints are applied to the array geometry for the same look direction, (r, z), the width of the mainlobe would be invariant from that of the single constraint MV in the presence of array tilt alone (refer to Fig. 3). When control of the mainlobe width is also desirable to reduce sampling requirements and environmental mismatch, the MTC can easily be combined with the WNC as described below.

C. WNC plus MCM

The WNC is to impose an additional quadratic inequality constraint such that

$$\delta^2 \le G_{\mathbf{w}} = \frac{1}{\mathbf{w}^{\dagger}\mathbf{w}} \le \max(G_{\mathbf{w}}) = 1, \tag{8}$$

where $G_{\mathbf{w}}$ is the white noise gain (WNG) whose reciprocal is a measure of sensitivity to tolerance errors.[6] The constraint value δ^2 must be chosen less than or equal to the maximum possible WNG, $\max(G_{\mathbf{w}}) = 1$, which is attained for the conventional Bartlett weight vector, $\mathbf{w}_B$. The formulation of WNC plus MCM is to minimize the output power subject to both the MTC and WNG constraints,

$$\min_{\mathbf{w}_C} \mathbf{w}_C^{\dagger}\mathbf{R}\mathbf{w}_C \quad \text{subject to } \mathbf{w}_C^{\dagger}\mathbf{E} = \mathbf{d} \text{ and } G_{\mathbf{w}_C} \ge \delta^2. \tag{9}$$

The solution to the problem is the same as that of the MCM in Eq. (5), except the covariance matrix $\mathbf{R}$ is diagonally loaded,[12]

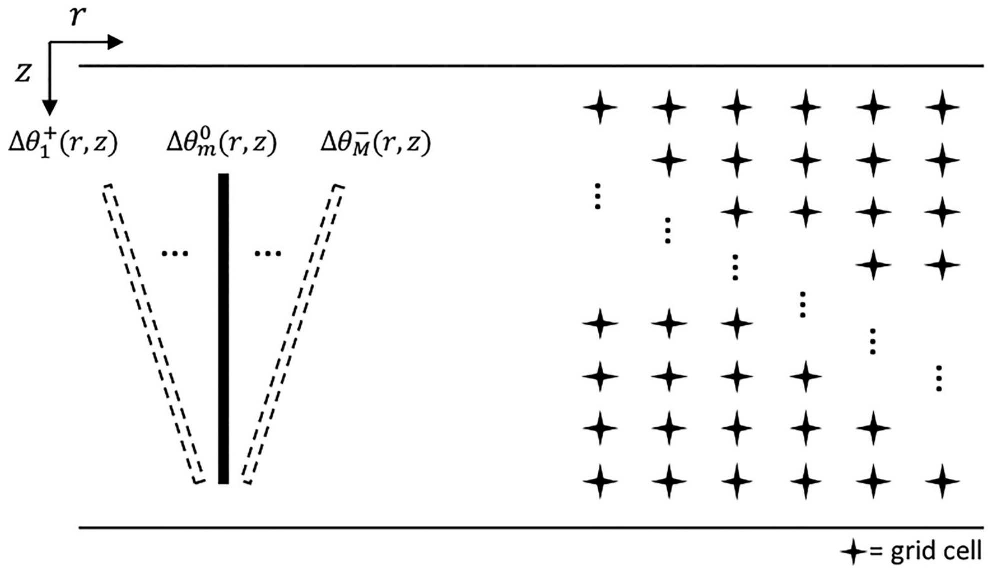

FIG. 1. Multiple tilt constraints (MTC) imposed on the vertical array. A positive angle ($\Delta\theta^+$) is assigned to a counter-clockwise rotation in the source-receiver plane. The constraint matrix $\mathbf{E}$ in Eq. (6) is composed of M replica vectors, $\mathbf{e}_{\Delta\theta}$, corresponding to various tilt angles between positive ($\Delta\theta^+$) and negative ($\Delta\theta^-$) values with no array tilt ($\Delta\theta_m^0 = 0°$) in the middle (thick line).

$$\mathbf{w}_C = (\mathbf{R}+\epsilon\mathbf{I})^{-1}\mathbf{E}\left[\mathbf{E}^\dagger(\mathbf{R}+\epsilon\mathbf{I})^{-1}\mathbf{E}\right]^{-1}\mathbf{d}^\dagger, \quad (10)$$

where $\mathbf{I}$ is the identity matrix. For each weight vector, the diagonal loading (ϵ) is iteratively increased from an initial value [e.g., $\epsilon_0 = 10\log(\mathrm{tr}(\mathbf{R})/N) - 40$ in dB scale where tr () denotes the trace of a matrix] until the WNG satisfies Eq. (8) [e.g., WNG $= 10\log(\delta^2)$ within ± 0.1 dB]. Note that δ^2 provides a parameterization between the robustness of the conventional Bartlett of Eq. (3) (WNG = 0 dB) and the interference-rejection capability of the pure MCM of Eq. (5) (WNG $= -\infty$ dB). Throughout this paper, we will use WNG $= -3$ dB as a trade-off between environmental robustness and sidelobe control.

III. THE SAVEX15 EXPERIMENT

The Shallow-water Acoustic Variability EXperiment (SAVEX15)[14] was conducted in the northeastern East China Sea in May 2015 using the R/V *Onnuri*. The experimental site had a nearly flat sandy bottom and a water depth of approximately 100 m. Both fixed and towed source transmissions (>3 kHz) were carried out to two bottom-moored vertical line arrays (VLAs) over ranges of 1–10 km. To evaluate the performance of various MFP processors, we revisit the dataset from a source-tow event analyzed in a recent paper[11] that revealed the significant impact of array tilt even on the Bartlett MFP.

The schematic of the experiment during the source-tow run is illustrated in Fig. 2(a). The bottom-moored VLA consisted of 16 elements ($N = 16$) spanning a 56.25 m aperture with 3.75-m element spacing, covering about half of the water column (from 25 to 81 m) in about 100-m deep shallow water. The SSP (solid line) is an average of CTD (conductivity, temperature, and depth) casts collected on JD 145 (May 25), featuring an asymmetrical underwater sound channel with the channel axis at about 40 m depth. The geoacoustic bottom parameters for modeling are compressional speed $c_b = 1800$ m/s, density $\rho = 1.97$ g/cm^3, and attenuation $\alpha_b = 0.94$ dB/λ.

The R/V *Onnuri* was circling around the VLA counterclockwise, mostly at a speed of 3 kn (1.5 m/s) at various ranges of 1.8–3.6 km from the VLA at the origin. The global positioning system (GPS) ship track is shown in Fig. 2(b) for the entire 4-h period (15:45–19:35 UTC), and the solid triangle and square denote the start and end points on the track, respectively. Although no tilt sensor was attached to the VLA, the array tilt was separately estimated from the self-calibrated array invariant method,[15] as shown in Fig. 5(a). A representative example at $r = 2.7$ km range (green circle, 19:19 UTC) with the array tilt ($\Delta\theta = +3.3°$) is selected for evaluation of various MFP processors in Sec. V A.

IV. MFP SIMULATIONS

For reference, the performance of various MFP processors is first simulated for the ideal case (i.e., perfect match), where the same environmental model and array geometry (no tilt) are assumed for calculating the source field and the replica fields. Moreover, the sampling is chosen such that the ambiguity surfaces are sampled at the exact source position. Then, three sources of parameter mismatch (environment, array geometry, and grid sampling) are introduced to investigate their sensitivities. We assume a perfectly known covariance matrix with spatially white sensor noise: $\mathbf{R} = \sigma_s^2 \mathbf{e}(r_s, z_s)\mathbf{e}^\dagger(r_s, z_s) + \sigma_n^2\mathbf{I}$, where σ_s^2 is the source strength and σ_n^2 is the level of sensor noise.[1]

A. No mismatch

With perfect environment model and array geometry (no tilt), range/depth ambiguity surfaces for five different

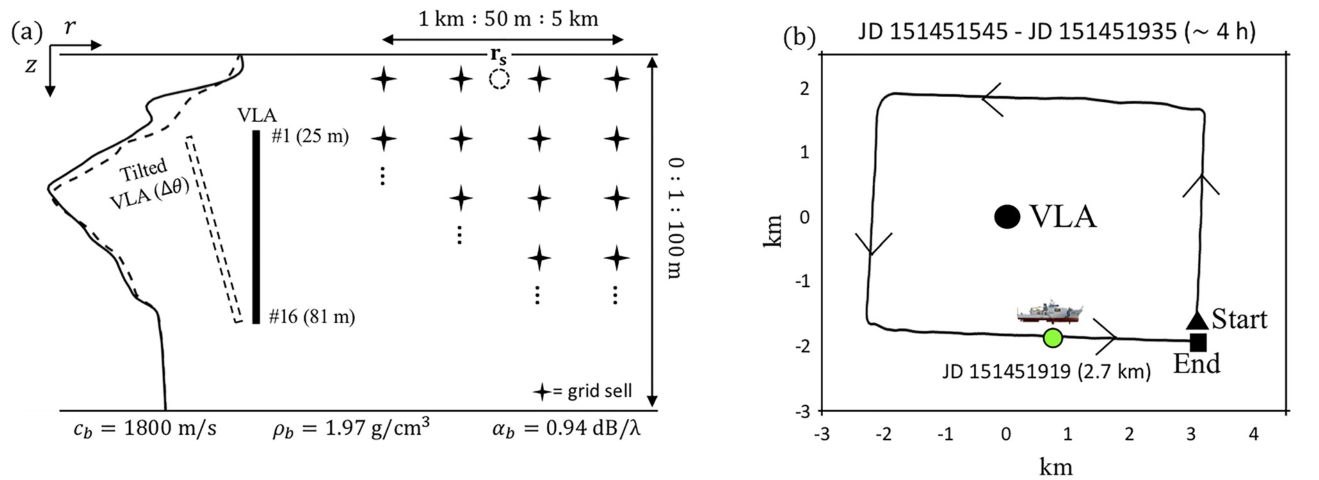

FIG. 2. (Color online) Schematic of the experiment conducted on JD 145 (May 25) during the source-tow run using the R/V *Onnuri*. (a) A 16-element, 56-m long, bottom-moored VLA in about 100-m deep water recorded the ship-radiated noise (200–500 Hz). The SSP (solid line) is an average of CTD profiles collected on JD 145, and the geo-acoustic parameters are shown in the bottom. For simulations in Sec. IV (see Fig. 3), three different types of mismatch are included (dashed): environment (SSP), system (array tilt), and grid sampling for a source at $\mathbf{r}_s$. (b) GPS ship track of the R/V *Onnuri* circling around the VLA at the origin counter-clockwise, mostly at a speed of 1.5 m/s for about a 4-h period (15:45–19:35 UTC). The green circle denotes the ship at 2.7 km range (JD 151451919) selected for evaluation of various MFP processors in Sec. V A (see Fig. 4).

MFP processors are shown in Fig. 3 (left column) from the top: Bartlett, MV, WNC, MTC, and MTC-WNC. A 200-Hz source is positioned at 4 km range and 5 m depth with a source level (σ_s^2) of 180 dB, and the sensor noise level (σ_n^2) is 100 dB. Given the average transmission loss of about 60 dB, the average SNR per hydrophone is 20 dB. Assuming a range-independent environment, the SSP (solid line) and geo-acoustic parameters in Fig. 2(a) are used to generate replica fields via the KRAKEN normal mode program.[16] The ambiguity surfaces cover the range interval 1–5 km and depth interval 0–100 m, with the grid cell size of 50-m in range and 1-m in depth ($\Delta r = 50$ m, $\Delta z = 1$ m). For MTC, a five-point tilt constraint ($M = 5$) is applied at tilt angles, $-4^\circ, -2^\circ, 0^\circ, +2^\circ$, and $+4^\circ$. The circles and squares denote the true source position and the global peak, respectively. In addition, the region around the global peak for no mismatch is expanded.

In the absence of mismatch, all five processors have a global peak (□) at the correct source position (○). However, the Bartlett ambiguity surface (top) exhibits a significant sidelobe structure. In contrast, the MV uniquely locates the source with a high resolution and sidelobe control. The MV and WNC both have excellent sidelobe suppression performance, but the WNC has a broader mainlobe controlled by the WNG constraint (δ^2). It is apparent that (1) MTC is equivalent to MV and (2) MTC-WNC is almost identical to WNC, indicating that the multiple tilt constraints did not affect the outcome of the corresponding processor with a single constraint in the absence of mismatch.

B. In the presence of mismatch

To illustrate the robustness of the MTC with respect to the array geometry, the vertical array is tilted by $\Delta\theta = +3^\circ$, similar to the experimental data ($\Delta\theta = +3.3^\circ$) analyzed in Sec. V A. The ambiguity surfaces obtained in this case are shown in the middle column of Fig. 3. Clearly, the Bartlett, MV, and WNC (top three) that did not take into account the perturbation in array geometry for such a large tilt failed to unambiguously localize the source. Rather, the global peaks (□) appear toward the bottom at around 2.1 km range, while the MV shows the extreme sensitivity to mismatch with a significant sidelobe structure compared to the case of perfect match (left column). On the other hand, the MTC and MTC-WNC (bottom two) both uniquely localize the source with excellent sidelobe suppression. In particular, the MTC is insensitive to the array tilt provided the tilt angle is within the bounds of the constraints (i.e., $|\Delta\theta| \le 4^\circ$). The MTC-WNC also shows a mainlobe width comparable to that of the WNC without mismatch (left column).

Next, we consider a more realistic scenario with all three types of parameter mismatch present, resulting from a slight perturbation in the SSP and the array tilt ($\Delta\theta = +3^\circ$) for a source located in the middle of a grid cell, as depicted in Fig. 2(a) (dashed). The ambiguity surfaces in this case are shown in the right column of Fig. 3. Since the top three (Bartlett, MV, and WNC) were unable to yield a unique source position even with the array tilt alone (middle column), it would not be meaningful to discuss their performance with additional mismatches. However, the MTC and MTC-WNC (bottom two) still uniquely localize the source, albeit with several prominent sidelobes. It is also interesting to note that the width of the MTC mainlobe can be increased in the presence of environmental mismatch. In summary, the MTC-WNC can provide the most robust performance with a wider mainlobe and sidelobe suppression in the presence of environmental, array tilt, and sampling mismatch altogether. In the following, these findings will be confirmed using experimental data.

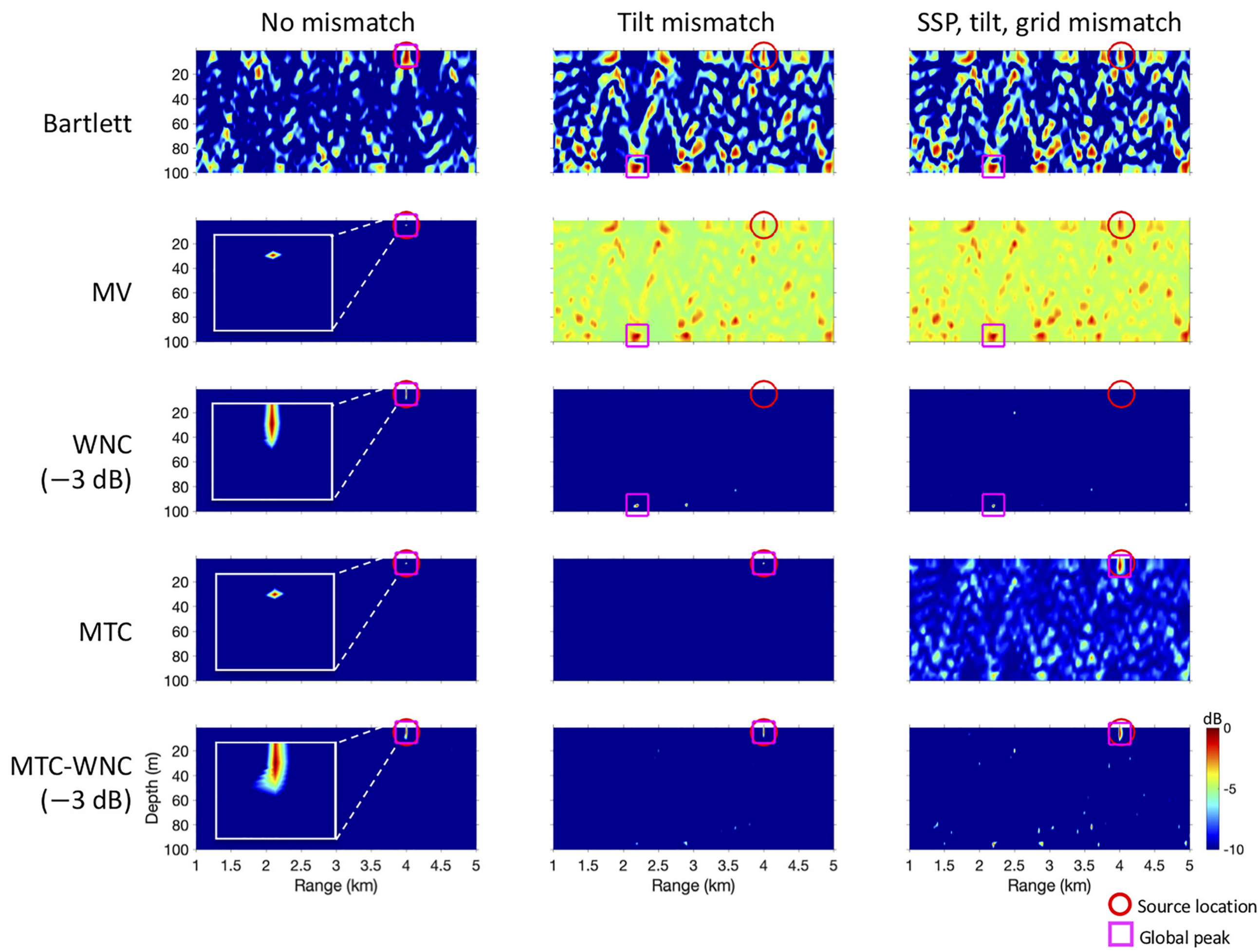

FIG. 3. (Color online) Simulated performance of various MFP processors for a 200-Hz source at range 4 km and depth 5 m: Bartlett, MV, WNC, MTC, and MTC-WNC. (Left column) No mismatch. (Middle) Array tilt mismatch ($\Delta\theta = +3°$). (Right) Mismatch in SSP, array tilt ($\Delta\theta = +3°$), and grid sampling [see Fig. 2(a)]. The region around the global peak for no mismatch (left column) is expanded. For MTC, a five-point tilt constraint ($M = 5$) is applied at tilt angles, $-4°, -2°, 0°, +2°$, and $+4°$. The circles and squares denote the true source position and the global peak, respectively. The MTC-WNC (bottom right) provides the most robust performance with a wider mainlobe and sidelobe suppression in the presence of environmental, array tilt, and sampling mismatch altogether. The dynamic range is 10 dB.

V. EXPERIMENTAL RESULTS

To evaluate the robustness of the various MFP processors with the SAVEX15 data, the range-independent acoustic environment used for the simulation in Sec. IV A is adopted to generate the replica fields. In fact, the same environmental model provided a good performance for the conventional Bartlett MFP for a small array tilt (e.g., $|\Delta\theta| < 1.3°$) in Ref. 11, suggesting that it reasonably captures the actual propagation environment. Still, some unknown environmental mismatch exists as well as array tilt. We will employ the same five-point constraints for MTC ($M = 5$), WNG $= -3$ dB for WNC, and grid sampling used in simulations. First, we analyze a representative example with a large array tilt in detail and then present the overall performance of tracking the ship during the entire 4-h source-tow event as depicted in Fig. 2(b). The MV processor is excluded in the following analysis due to its high sensitivity to mismatch that is inevitable in real data.

A. MFP with array tilt

The ambiguity surfaces obtained by the four different processors are shown in Fig. 4 when the R/V *Onnuri* was at 2.7 km range (green circle) in Fig. 2(b): (a) Bartlett, (b) WNC, (c) MTC, and (d) MTC-WNC. The corresponding array tilt was large with $\Delta\theta = +3.3°$, separately estimated from the array invariant approach.[11,15] The observation time window to construct the sample covariance matrix ($\hat{\mathbf{R}}$) was $T = 2$ s, and the FFT length of each snapshot was 16 384 samples (≈160 ms) with a Kaiser window of $\alpha = 2.5$ and 50% overlap between successive FFTs, resulting in $L = 23$ snapshots with a FFT bin width of 6.1 Hz. The sampling frequency was 100 kHz. It should be pointed out that the 2-s time window was chosen carefully for two reasons. First, it is consistent with our earlier papers[11,15] for fair comparisons in Figs. 4 and 5. Second, for the ship speed of 3 kn (1.5 m/s), the radial travel distance is 3 m over $T = 2$ s, which is less than the wavelength at the center frequency 350 Hz (4 m).

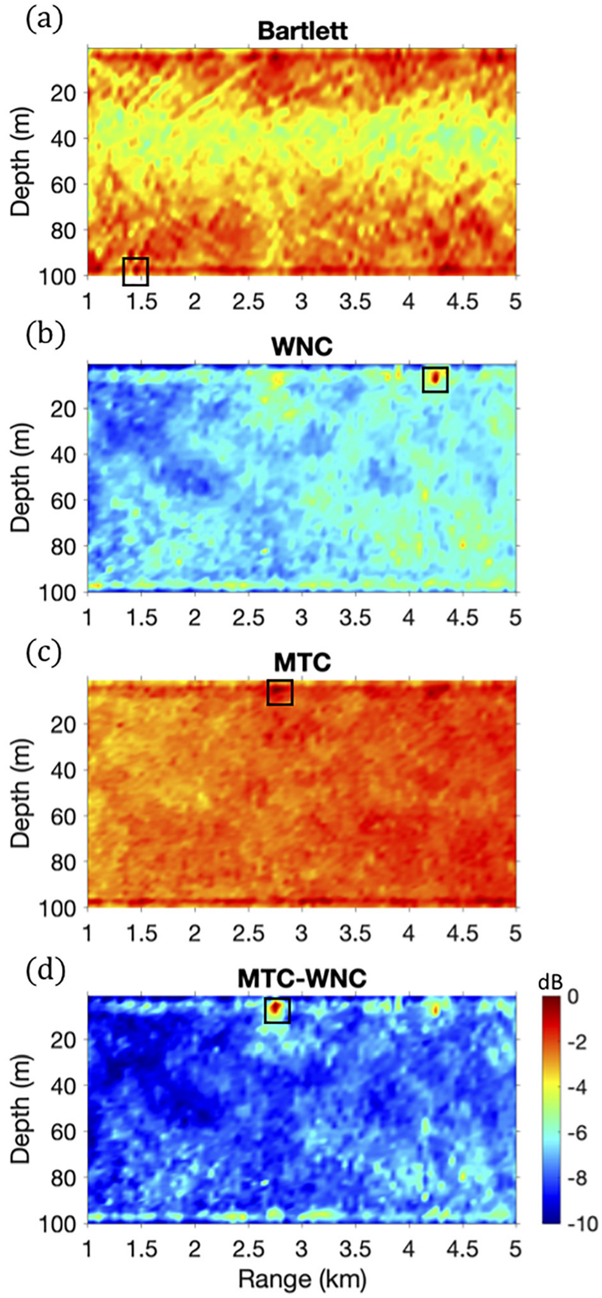

FIG. 4. (Color online) Ambiguity surfaces obtained with the R/V *Onnuri* at 2.7 km range depicted in Fig. 2(b) (green circle) for the (a) Bartlett, (b) WNC, (c) MTC, and (d) MTC-WNC. The array tilt was $\Delta\theta = +3.3°$. The sample covariance matrix $(\hat{\mathbf{R}})$ was constructed from a 2-s window of the ship noise (200–500 Hz), and the power outputs were incoherently averaged across the bandwidth at 10 Hz intervals, yielding the global peaks (□) either toward the surface or the bottom. Although (c) MTC has the global peak (2.7 km) close to the source range near the surface (5 m), the sidelobe/background levels are very high, within 2 dB from the mainlobe. Similar to Fig. 3 (right column), (d) MTC-WNC provides the best localization performance with a satisfactory sidelobe control in the presence of both unknown environmental mismatch and array tilt.

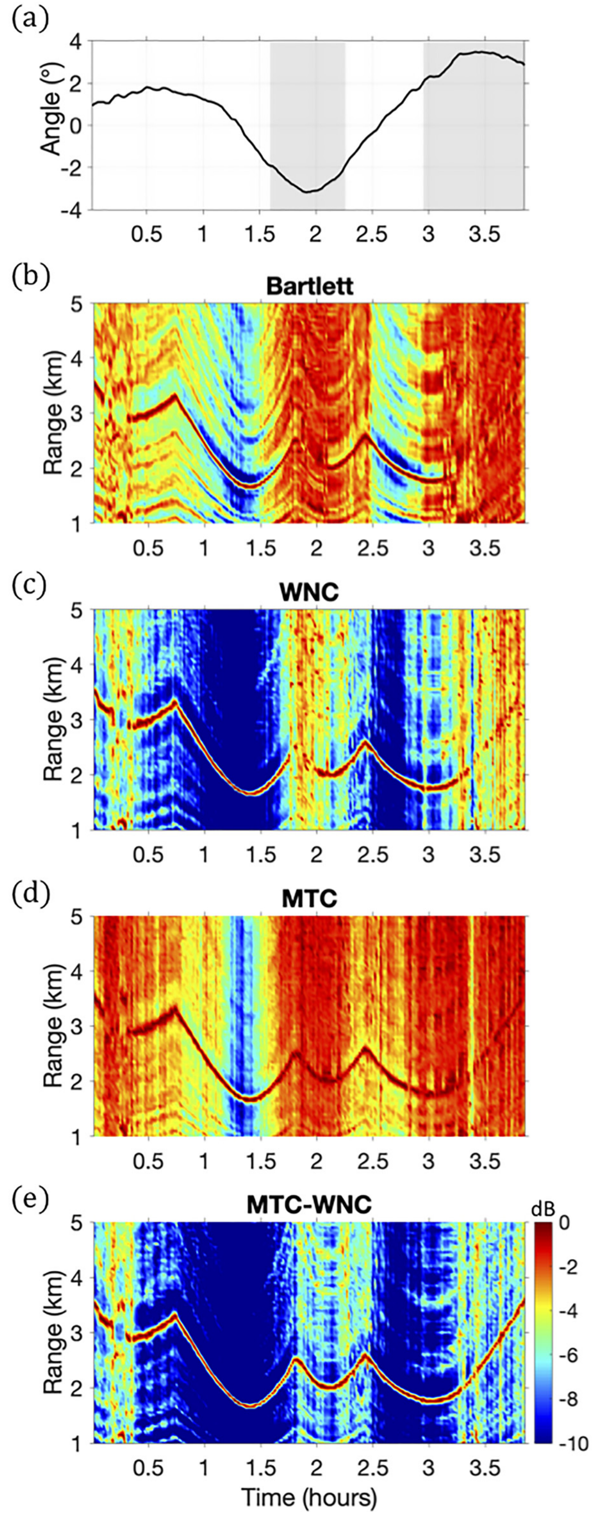

FIG. 5. (Color online) Range ambiguity at the estimated source depth [see Fig. 6(b)] for the entire 4-h period as depicted in Fig. 2(b), obtained by the (b) Bartlett, (c) WNC, (d) MTC, and (e) MTC-WNC. (a) Array tilt is separately estimated from the array invariant (Refs. 11, 15), and the shaded areas denote the period of large tilt angles, $|\Delta\theta| \geq 2°$. The tracking performance of all processors except the MTC-WNC has deteriorated severely in those regions. However, (c) WNC has a significantly better sidelobe suppression performance than the other two (Bartlett and MTC) outside the regions, comparable to the MTC-WNC. (e) MTC-WNC consistently shows the best localization performance in the presence of even unknown environmental mismatch and a large array tilt with superior sidelobe control.

Then the moving ship can be treated as quasi-stationary for MFP.[17] The outputs are incoherently averaged across the bandwidth (200–500 Hz) at 10 Hz intervals, and the global peaks are denoted by squares (□).

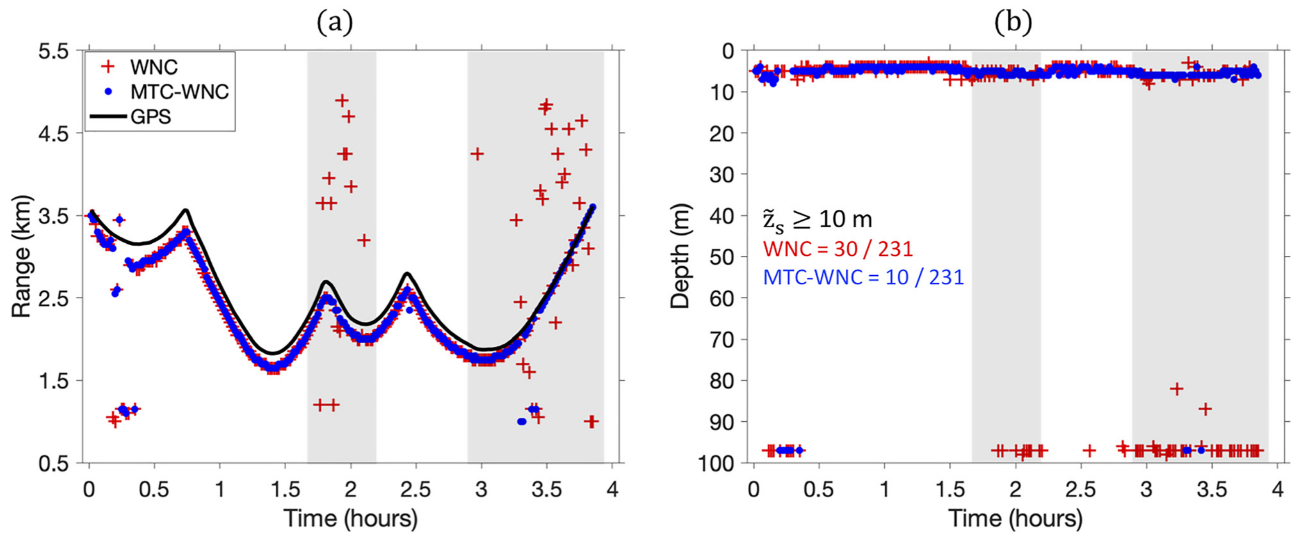

FIG. 6. (Color online) (a) Range estimate of the R/V *Onnuri* over the 4-h period, for the WNC (+) and MTC-WNC (•). The solid line indicates the ship GPS. (b) The corresponding depth estimate. The number of samples whose estimated depth is deeper than 10 m (i.e., bottom) is 10 out of 231 for the MTC-WNC, compared to 30 for the WNC. Note that most of the WNC errors occur in the shaded areas.

As observed in simulation results of Fig. 3 (right column), both (a) Bartlett and (b) WNC failed to localize the source uniquely in Fig. 4. Nevertheless, (b) WNC has a significantly better sidelobe suppression performance than (a) Bartlett, albeit with its global peak shifted to a longer range (4.2 km). While (c) MTC shows a global peak at 2.7 km that is close to the source range near the surface (5 m), the sidelobe/background levels are too high, within 2 dB from the mainlobe peak. In consistent with the simulations, (d) MTC-WNC does provide the best localization performance with a satisfactory sidelobe control in the presence of both unknown environmental mismatch and a large array tilt.

B. MFP performance of tracking the ship

In this section we investigate the overall performance of tracking the R/V *Onnuri* during the entire 4-h period. The range ambiguity at the estimated source depth is shown in Fig. 5: (b) Bartlett, (c) WNC, (d) MTC, and (e) MTC-WNC. The vertical axis denotes the range (km), and the horizontal axis indicates the time (hours). The 2-s window of the ship-radiated noise (i.e., 25–27 s) was selected every minute, generating a total 231 discrete samples. The array tilt estimated from the self-calibrated array invariant[11] is included in Fig. 5(a) to illustrate its impact on MFP. While the tilt angles are less than 4°, the shaded areas denote the period of large tilt angles, $|\Delta\theta| \geq 2°$.

The performance of all processors except (e) MTC-WNC has deteriorated significantly in those shaded areas. It is interesting to note that (d) MTC outperforms (b) Bartlett in terms of range tracking during the entire period, but still suffers from high sidelobe levels resulting from environmental mismatch. Similar to Fig. 4, (c) WNC has a significantly better sidelobe suppression performance than the other two (Bartlett and MTC). In fact, for small tilt angles (outside the shaded areas), the WNC performance is comparable to that of the MTC-WNC, indicating that the small array tilt can be treated as mild environmental mismatch. In summary, (e) MTC-WNC consistently provides the best localization performance in the presence of array tilt and unknown environmental mismatch with superior sidelobe control.

Finally, the estimated range and depth from the global peak (□) in the ambiguity surface (e.g., Fig. 4) are displayed in Fig. 6, for the WNC (+) and MTC-WNC (●). The solid line in Fig. 6(a) indicates the ship GPS. While the MTC-WNC ranges (●) closely follow the ship GPS except a few outliers, they are consistently underestimated (i.e., below the ship GPS), which is most likely due to the mismatch in bathymetry.[18] In Fig. 6(b), the number of samples whose estimated depth is deeper than 10 m (i.e., bottom) is 10 out of 231 cases for the MTC-WNC, compared to 30 for the WNC. Moreover, most of the WNC errors in range and depth occur in the shaded areas as expected.

VI. CONCLUSIONS

Traditional MFPs such as the linear Bartlett and the high-resolution MV have severe problems in relation to sidelobe suppression and robustness to environmental mismatch, respectively. As a compromise, the WNC has been developed to mitigate some environmental mismatch while maintaining its localization and sidelobe control. An additional important source of mismatch is the array tilt that has not received much attention in spite of its significant impact, especially for a large array tilt observed in shallow water (e.g., $|\Delta\theta| > 2°$). Here, the special MCM (MTC) was designed to broaden the boundaries of the array geometry, while simultaneously widening the mainlobe using the WNC. The adaptive MFP that combined the MTC and the WNC (MTC-WNC) demonstrated significant improvement in robustness to both environmental mismatch and a large array tilt through both simulations and experimental data.

ACKNOWLEDGMENT

This work was supported by the U.S. Office of Naval Research under Award No. N00014-17-1-2101.

[1]A. B. Baggeroer, W. A. Kuperman, and P. N. Mikhalevsky, "An overview of matched field methods in ocean acoustics," IEEE J. Oceanic Eng. **18**, 401–424 (1993).

[2]M. D. Collins and W. A. Kuperman, "Focalization: Environmental focusing and source localization," J. Acoust. Soc. Am. **90**, 1410–1422 (1991).

[3]H. Schmidt, A. B. Baggeroer, W. A. Kuperman, and E. K. Scheer, "Environmentally tolerant beamforming for high-resolution matched field processing: Deterministic mismatch," J. Acoust. Soc. Am. **88**, 1851–1862 (1990).

[4]A. B. Baggeroer, W. A. Kuperman, and H. Schmidt, "Matched field processing: Source localization in correlated noise as an optimum parameter estimation problem," J. Acoust. Soc. Am. **83**, 571–587 (1988).

[5]J. L. Krolik, "Matched-field minimum variance beamforming in a random ocean channel," J. Acoust. Soc. Am. **92**, 1408–1419 (1992).

[6]H. Cox, R. M. Zeskind, and M. M. Owen, "Robust adaptive beamforming," IEEE Trans. Acoust. Speech Sign. Process. **10**, 1365–1376 (1987).

[7]N. O. Booth, A. T. Abawi, P. W. Schey, and W. S. Hodgkiss, "Detectability of low-level broad-band signals using adaptive matched-field processing with vertical aperture arrays," IEEE J. Ocean. Eng. **25**, 296–313 (2000).

[8]H. Cox and R. Pitre, "Robust DMR and multi-rate adaptive beamforming," in *IEEE Proceedings of the 31st Asilomar Conference on Signals, Systems and Computers* (1997), pp. 920–924.

[9]J. L. Krolik, "The performance of matched-field beamformers with Mediterranean vertical array data," IEEE Trans. Sign. Process. **44**, 2605–2611 (1996).

[10]Seongil Kim, W. A. Kuperman, W. S. Hodgkiss, H. C. Song, G. F. Edelmann, and T. Akal, "Robust time reversal focusing in the ocean," J. Acoust. Soc. Am. **114**, 145–157 (2003).

[11]G. Byun, H. C. Song, and J. S. Kim, "Performance comparisons of array invariant and matched field processing using broadband ship noise and a tilted vertical array," J. Acoust. Soc. Am. **144**, 3067–3074 (2018).

[12]J. Q. D. Tran and W. S. Hodgkiss, "Matched-field processing of 200-Hz continuous wave (CW) signals," J. Acoust. Soc. Am. **89**, 745–755 (1991).

[13]K. L. Gemba, S. Nannuru, P. Gerstoft, and W. S. Hodgkiss, "Multi-frequency sparse Bayesian learning for robust matched field processing," J. Acoust. Soc. Am. **141**, 3411–3420 (2017).

[14]H. C. Song, C. Cho, W. S. Hodgkiss, S. Nam, S. Kim, and B. Kim, "Underwater sound channel in the northeastern East China Sea," Ocean Eng. **147**, 370–374 (2018).

[15]G. Byun, C. Cho, H. C. Song, J. S. Kim, and S. Byun, "Array invariant-based calibration of array tilt using a source of opportunity," J. Acoust. Soc. Am. **143**, 1318–1325 (2018).

[16]M. B. Porter, "The acoustics toolbox," http://oalib.hlsresearch.com/Modes/AcousticsToolbox/ (Last viewed 2/15/2020).

[17]H. C. Song, "Performance bounds for passive localization of a moving source for ocean acoustics," Ph.D. thesis, MIT, Cambridge, MA (1990).

[18]G. L. D'Spain, J. J. Murray, W. S. Hodgkiss, N. O. Booth, and P. W. Schey, "Mirages in shallow water matched field processing," J. Acoust. Soc. Am. **105**, 3245–3265 (1999).